

Manipulation of internal blockage in triangular triple quantum dot

Yue Qi(齐月) and Jian-Hua Wei(魏建华)

Citation: Chin. Phys. B, 2024, 33 (**5**): 057301. DOI: 10.1088/1674-1056/ad2d54
Journal homepage: http://cpb.iphy.ac.cn; http://iopscience.iop.org/cpb

What follows is a list of articles you may be interested in

Chiral current regulation and detection of Berry phase in triangular triple quantum dots

Yue Qi(齐月), Yi-Ming Liu(刘一铭), Yuan-Dong Wang(王援东), Jian-Hua Wei(魏建华), and Zhen-Gang Zhu(朱振刚)
Chin. Phys. B, 2023, 32 (**8**): 087304. DOI: 10.1088/1674-1056/acd36c

Delayed response to the photovoltaic performance in a double quantum dots photocell with spatially correlated fluctuation

Sheng-Nan Zhu(祝胜男), Shun-Cai Zhao(赵顺才), Lu-Xin Xu(许路昕), and Lin-Jie Chen(陈林杰)
Chin. Phys. B, 2023, 32 (**5**): 057302. DOI: 10.1088/1674-1056/ac8e97

Thermoelectric signature of Majorana zero modes in a T-typed double-quantum-dot structure

Cong Wang(王聪) and Xiao-Qi Wang(王晓琦)
Chin. Phys. B, 2023, 32 (**3**): 037304. DOI: 10.1088/1674-1056/ac92d3

Real-time dynamics in strongly correlated quantum-dot systems

Yong-Xi Cheng(程永喜), Zhen-Hua Li(李振华), Jian-Hua Wei(魏建华), and Hong-Gang Luo(罗洪刚)
Chin. Phys. B, 2023, 32 (**12**): 127302. DOI: 10.1088/1674-1056/acf448

Nonlinear optical rectification of GaAs/$Ga_{1-x}Al_xAs$ quantum dots with Hulthén plus Hellmann confining potential

Yi-Ming Duan(段一名) and Xue-Chao Li(李学超)
Chin. Phys. B, 2023, 32 (**1**): 017303. DOI: 10.1088/1674-1056/ac70bf

---

Manipulation of internal blockage in triangular triple quantum dot

Yue Qi(齐月) and Jian-Hua Wei(魏建华)†

Department of Physics, Renmin University, Beijing 100876, *China*

(Received 16 October 2023; revised manuscript received 4 February 2024; accepted manuscript online 27 February 2024)

We utilize the calculation of hierarchical equations of motion to demonstrate that the spin-dependent properties between adjacent quantum dots (QDs) can be changed by breaking the internal symmetry configuration, corresponding to the inversion of dominant chiral states. In the linear triple quantum dots (LTQDs) connected to two electron reservoirs, we can observe that the blockage appears at the triangle triple quantum dots (TTQDs) by gradually increasing the coupling strength between next-nearest double QDs. When the initial coupling between LTQDs has altered, the internal chiral circulation also undergoes the corresponding transform, thus achieving qualitative regulation and detection of the blocking region. We also investigate the response of the chiral circulation to the dot–lead coupling strength, indicating the overall robust chiral circulation of the TTQDs frustration.

Keywords: quantum dots, chiral topology blocking

PACS: 73.21.La, 75.10.Pq, 64.70.Tg **DOI:** 10.1088/1674-1056/ad2d54

1. Introduction

With the invention of semiconductor transistor and in-depth research on device miniaturization, quasi zero-dimensional nanostructures of quantum dots (QDs) have become a research hotspot.[1–4] Electrons in QDs have the characteristics of electron level separation and charge quantization. The successful manufacture of a QD system provides a practical value for theoretical research.[5–8] The symmetry and exchange interaction of the internal isolated system and quantum states can be controlled by tuning the gate voltage and Coulomb repulsion energy.[9–11]

In recent years, as the triangle triple quantum dots (TTQDs) are the smallest elementary structures with topological phenomena, some unique internal characteristics such as chirality states, chiral currents, mixed valence bonds, and Kondo effect are being studied by theoretical researchers.[12–15] In addition to the spin freedom, the system has an additional spin chirality term. The ground state of TTQDs can be composed of chirality states because of their spin frustration, which makes the study of chiral circulation and chirality states in TTQDs a more important factor.

As early as 2002, Tatara *et al.* discovered that in strong coupling, the anomalous Hall effect (AHE) originates from non-trivial spin chiral configurations.[16–18] By studying the exchange among three local spins, an additional geometric (Berry) phase factor of traveling electron is found when those spins subtend solid angle Ω. This serves as an internal effective magnetic field generated by the non-coplanar local spin which elicits the anomalous Hall effect (AHE) and chiral current.[19–22] The effective field can be represented by chirality $\hat{\boldsymbol{S}}_1 \cdot (\hat{\boldsymbol{S}}_2 \times \hat{\boldsymbol{S}}_3)$, which makes the internal field generated by spin chirality as a factor in the charge dynamics as the external field.[7,23,24] Two chiral states were found in the three-spins ring, both of which were driven by the chirality term and controlled by the spin Josephson effect. This effect is due to the non-commutativity of spin exchange breaking the time-reversal symmetry. The electron wave function must appear coherent superposition, with internal circulation proportional to the spin chirality.[25,26]

Recently, the chiral circulation has been applied to practical TTQDs system. When the relative coupling strength between the QDs is changed, the system symmetry breaks to induce two chiral states and internal chiral circulations. It is proposed for the first time that the chiral state and Berry phase can be controlled by pure electricity to manipulate qubit.[27]

From the results of the above-mentioned research, it can be seen that the basic structure exhibits spin frustration no matter whether it is conduction electrons or holes. With the additional phase factor, it can greatly reduce energy consumption and be applied to the latest microelectronics research. Quantum computers follow the logic of quantum mechanics, have better performance than classical computers to solve certain problems that classical computers cannot. With the continuous progress of science and technology, a multi-quantum dot system on a semiconductor heterojunction has successfully prepared in experiment, which provides an ideal platform for in-depth study of multi-body physics, and also provides a solid foundation for solid-state quantum computing devices. The model has become an important research object of mesoscopic nanosystems.

This paper is based on the TTQDs, in which the tunneling between adjoining QDs are set as t_{12} and t_{13}, and the side $\mathrm{QD}_{2/3}$ is t as shown in Fig. 1(a). Two leads are symmetrically coupled to QD_2 and QD_3 with hybridization $\Gamma_{\mathrm{L}} = \Gamma_{\mathrm{R}} = \Delta =$

†Corresponding author. E-mail: wjh@ruc.edu.cn

© 2024 Chinese Physical Society and IOP Publishing Ltd

0.025 meV. The inversion of the chiral state is further found to be closely related to symmetry. We reduce the system with $t_{12} = t_{13} = t_0$, and set $t = 0$ as a chain of linear triple quantum dots (LTQDs) without chiral circulation. When t gradually increases, the structure becomes a triangular ring causing the chiral circulation to appear and reverse. As the distance between QD_2 and QD_3 gets closer, double spins on each QD change from the ferromagnetic (FM) to the anti-ferromagnetic (AFM) interaction with reversing the dominant chiral state.

When $t_{12} = t_{13} = t$ in TTQDs form an C_{3v} equilateral triangle structure, the chiral current (J_c) and the corresponding conduction current (J_t) will appear in spin frustration. The spin frustration has transformation as $t_{12} \neq t_{13}$ in the initial LTQDs to break left-right mirror. Further study also finds that the dot–lead coupling also affects the internal chiral circulation and spin correlation, while it has little impact on the overall trend of the spontaneous symmetry breaking.[28–35]

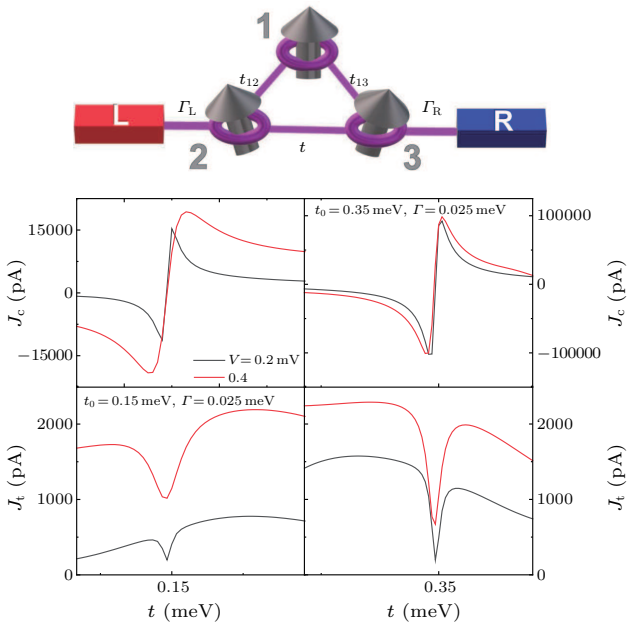


Fig. 1. (a) Structural diagram of TTQDs connecting two reservoirs, in which the coupling strength between QD_2 and QD_3 is set to t, which are coupled to the left and right electron reservoirs with $\Gamma_{L/R} = \Delta = 0.025$ meV, respectively, while the coupling strengths between QD_1 and $QD_{2/3}$ are set to t_{12} and t_{13} respectively. The system is half-filling, with each QD occupied by a spin $S = 1/2$. The parameters are all in meV, the temperature is set as $k_BT = 0.05$ and $\varepsilon = -0.5$, $U = 1.0$. (b)–(e) When the initial structure is set to a symmetric mirror TTQD, $t_{12} = t_{13} = t_0$, the chiral current J_c and conduction current J_t are functions of t. The black line represents the bias voltage of 0.2, the red solid line is $V = 0.4$ mV of the J_c and J_t with the coupling strength t between QD_2 and QD_3. The initial structure is $t_0 = 0.15$ in (b) and (d), while in (c) and (e) represents the situation at $t_0 = 0.35$.

2. Theoretical methods

We mainly use the Anderson impurity model to describe a quantum open system. The total Hamiltonian can be written as

$$H_T = H_{dots} + H_{res} + H_{coup}. \tag{1}$$

The Hamiltonian of dots can be expressed as

$$H_{dots} = \sum_{j,k=1}^{3} \sum_{s=\uparrow,\downarrow} t_{jk} \hat{d}_{js}^{\dagger} \hat{d}_{ks} + \sum_{j=1}^{3} U_j \hat{n}_{j\uparrow} \hat{n}_{j\downarrow}, \tag{2}$$

in which $\hat{d}_{js}^{\dagger}$ and $\hat{d}_{js}$ represent the generation and annihilation operator of an electron that occupies the on-dot molecular orbital. The t_{ij} $(i, j = 1,2,3)$ represents the coupling strength between QD_i and QD_j.

The dot–lead coupling term is

$$H_{coup} = \sum_{\kappa s} (t_{L2} \hat{c}_{L\kappa s}^{\dagger} \hat{d}_{2s} + t_{R3} \hat{c}_{R\kappa s}^{\dagger} \hat{d}_{3s} + \text{H.c.}), \tag{3}$$

where $t_{L2} = t_{R3} = \Gamma_L = \Gamma_R = \Delta$; and $\hat{c}_{\alpha\kappa s}^{\dagger}$ represents the generation operator of the electron on $\alpha = L/R$ leads. Through the previous research,[7,36,37] it is possible to perturb the transition coupling t of H_{dots} to obtain the third-order term, and the effective Hamiltonian about t–J–χ is[25,26]

$$\begin{aligned} H_{eff} = & -t(1-n) \sum_{jk,s} (\hat{d}_{js}^{\dagger} \hat{d}_{ks} + \text{H.c.}) \\ & + J \sum_{j<k} \left(\hat{\boldsymbol{S}}_j \hat{\boldsymbol{S}}_k - \frac{1}{4} \hat{n}_j \hat{n}_k \right) + \chi \hat{\boldsymbol{S}}_1 (\hat{\boldsymbol{S}}_2 \times \hat{\boldsymbol{S}}_3). \end{aligned} \tag{4}$$

For simplicity, we set $\varepsilon = -U/2 = -0.5$ meV to keep TTQDs in the particle-hole symmetry in which each QD is half-filling with the occupation $n = 1$ and the first term reduces to zero. The second represents the Heisenberg exchange, with $J = 4t^2/U$. Here, $\chi = 24 t_{12} t_{13} t_{23} \sin(2\pi\phi/\phi_0)/U^2$ is the chiral factor, with chiral operator $\hat{\boldsymbol{S}}_1 \cdot (\hat{\boldsymbol{S}}_2 \times \hat{\boldsymbol{S}}_3)$.

The ground states of isolated TTQDs exhibit chirality and spin quadruple degeneracy with $S_{tot} = 3/2$. Adding bias will disrupt the reflection symmetry of the entire system, which results in the coupling between spin current and spin gauge field. In $S_z = -1/2$ sub-space, the quadruplet states degenerate into clockwise (CW) and counterclockwise (CCW) chiral states $|q_{\pm}^{-1/2}\rangle = \frac{1}{\sqrt{3}} (|\uparrow\downarrow\downarrow\rangle + e^{\pm\frac{i2\pi}{3}} |\downarrow\uparrow\downarrow\rangle + e^{\pm\frac{i4\pi}{3}} |\downarrow\downarrow\uparrow\rangle)$.

Notably, in $S_z = 1/2$, $|q_{\pm}^{1/2}\rangle$ just flips all the spins of $|q_{\pm}^{-1/2}\rangle$. Chiral current also comes out:[38]

$$\begin{aligned} \hat{J}_c &= -\frac{e}{\hbar} \left\langle \frac{\partial \hat{H}_{dots}}{\partial \phi} \right\rangle = -\frac{e}{\hbar} \frac{\partial F_{dots}}{\partial \phi} \\ &= -\frac{24e}{\hbar} \frac{t_{12} t_{13} t_{23}}{U^2} \hat{\boldsymbol{S}}_1 \cdot (\hat{\boldsymbol{S}}_2 \times \hat{\boldsymbol{S}}_3). \end{aligned} \tag{5}$$

It has been preliminarily proved that by changing the external bias and the coupling strength t_{ij} between QDs, the dominant chiral state will be reversed. The chiral circulation will undergo CW and CCW transformations, which is caused by internal blockage of TTQDs.[27] The chiral circulation in the TTQDs is obtained by the scalar spin chirality term. $\hat{\boldsymbol{S}}_1 \cdot (\hat{\boldsymbol{S}}_2 \times \hat{\boldsymbol{S}}_3)$ breaks the symmetry of TTQDs and causes the chiral degree of freedom to split. Among them, when the CW chiral state dominates, the entire circulation will show a CW current (−); otherwise, it will flow in the CCW direction (+).

Since two electron reservoirs in output are added, there will still be J_t at both ends. The J_t inside the system can be excited by external bias voltage or vertical magnetic flux. The electrons only move in the entire circulating current system. Along the ring, the bond current between any two QDs through the electrode α can be defined as

$$J_{\alpha=\mathrm{L/R}}(t) = \mathrm{i}\sum_{\mu s}\mathrm{tr}[\rho^{\dagger}_{\alpha\mu s}(t)\hat{d}_{us} - \hat{d}^{\dagger}_{\mu s}\rho^{-}_{\alpha\mu s}(t)] \tag{6}$$

with $\rho^{\dagger}_{\alpha\mu s} = (\rho^{-}_{\alpha\mu s})^{\dagger}$. The J_t can be obtained by solving the first-order auxiliary density matrix with the method of hierarchical equations of motion (HEOMs) and is further written as[39–41]

$$\hat{J}_t = J_{\alpha=\mathrm{L/R}}(t) = -\frac{e}{\hbar}\sum_{s}(t_{jk}\hat{d}_{js}\hat{d}^{\dagger}_{ks} - \mathrm{H.c.}). \tag{7}$$

The HEOM approach is used to investigate the properties of quantum dots in both equilibrium and non-equilibrium states via the reduced density operator, which has a universal formalism for an arbitrary system Hamiltonian. Thus, it can be used to accurately solve the three-impurity Anderson model.[36] The HEOM approach is established based on Feynman–Vernon influence functional path-integral theory[42,43] without any approximations, and is implemented with Grassmann algebra for fermion dissipations.[44] Basically, the HEOM method is non-perturbative for general quantum systems coupled to reservoir baths those satisfy Grassmann Gaussian statistics. The reduced density matrix and a set of auxiliary density matrices are the basic variables in the HEOM method. Based on the linear response theory of quantum open systems, the HEOM method can be used to obtain dynamical observables of strongly correlated quantum impurity systems accurately and efficiently.[39,45] At time t, the reduced system density operator, $\rho(t) = \mathrm{tr}_{\mathrm{res}}\rho_{\mathrm{T}}(t)$, is related to the initial value at time t_0 via the reduced Liouville-space propagator $\mathcal{G}(t,t_0)$ by

$$\rho(t) = \mathcal{G}(t,t_0)\rho(t_0). \tag{8}$$

The influence of bath enters the equations of motion with M exponentiations. The auxiliary density operators (ADOs) $\{\rho^{n}_{j} = \rho_{j_1\cdots j_n}\}$ are determined by the time derivative of the influence functional. The final form can be reduced to the following compact form (the detailed derivation process can be found in the supplementary material):

$$\begin{aligned}\dot{\rho}^{(n)}_{j_1\cdots j_n} = &-\Big(\mathrm{i}\mathcal{L} + \sum_{r=1}^{n}\gamma_{j_r}\Big)\rho^{(n)}_{j_1\cdots j_n} - \mathrm{i}\sum_{j}\mathcal{A}_{\bar{j}}\rho^{(n+1)}_{j_1\cdots j_n j}\\ &-\mathrm{i}\sum_{r=1}^{n}(-)^{n-r}\mathcal{C}_{j_r}\rho^{(n-1)}_{j_1\cdots j_{r-1}j_{r+1}\cdots j_n}.\end{aligned} \tag{9}$$

3. Results

3.1. Mirror symmetry TTQDs, $t_{12} = t_{13}$

In this section, we mainly study the TTQDs of left-right mirror symmetry in a strongly correlated system. The parameters can be set as $t_{12} = t_{13} = t_0$ meV and continuous regulation $t = t_{23}$. The temperature $k_{\mathrm{B}}T = 0.05$ meV, which is much higher than the Kondo temperature T_{k}. The independent TTQD is weakly coupled with the terminals at dot–lead hybridization $\Gamma_{\mathrm{L}} = \Gamma_{\mathrm{R}} = \Delta = 0.025$ meV $\ll t_0$, and the Coulomb repulsion energy is set to $\varepsilon = -U/2 = -0.5$ meV in the local magnetic moment region.

Figures 1(b)–1(e) show the variation of the internal J_c and J_t with t at $V = 0.2$ and 0.4 mV when the initial left-right mirror reflection symmetry of TTQDs is set to $t_0 = 0.15$ and 0.35 meV. It can be seen that when $t_0 = 0.15$ meV, the kink of the J_c and J_t also appears at $t = 0.15$ meV. At $t_0 = 0.35$ meV, the distortion point changes to $t = 0.35$ meV, indicating that the spin frustration region of the TTQD appears at the equilateral triangle symmetry of $t = t_0$. With the increase of bias voltage, the extremum of both currents will increase.

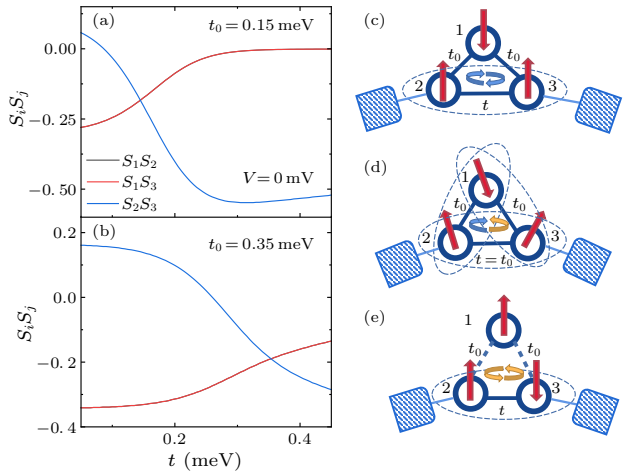


Fig. 2. (a) When $V = 0$ mV, the spin correlation coefficient $\langle S_iS_j\rangle$ between QD_i and QD_j $(i,j = 1$–$3)$ are as functions of coupling strength t between QD_2 and QD_3 at $t_0 = 0.15$ and $t_0 = 0.35$. Due to the symmetry of the TTQDs, there always exists $\langle S_1S_2\rangle = \langle S_1S_3\rangle$. (c)–(e) As t between QD_2 and QD_3 gradually increases, the interaction between three spins larger. When t is very small, the spin correlation between QD_2 and QD_3 is represented by a dashed circle as FM interaction in (c). At $t = t_0$, due to the equilateral symmetric structure, any two QDs are entangled with each other, causing spin interference and the superposition of internal CW and CCW chiral states in (d). At $t > t_0$, spin AFM coupling occurs, and dashed lines represent decoupling between side QDs and QD_1 in (e).

When $V = 0$, the spin correlation among three spins in TTQDs is further analyzed at $t_0 = 0.15$ meV and 0.35 meV, as shown in Fig. 2. Due to symmetry, there always exists $\langle S_1S_2\rangle = \langle S_1S_3\rangle$ without bias. In the $t/t_0 < 1$ region, because the coupling strength t is relatively small, the system is approximately an LTQDs chain in which local spins on side QD_2 and QD_3 are induced via an FM interaction.

As shown in Figs. 2(a)–2(f), when $t_0 = 0.15$ meV and $t = 0$ meV, the adjacent QDs couple via an AFM correlation

in this symmetric LTQDs, while the side QDs are in FM coupling, i.e., $\langle S_1S_2\rangle = \langle S_1S_3\rangle < 0, \langle S_2S_3\rangle > 0$. When TTQDs are in equilateral triangle at $t_{23} = t_0 = 0.15$ meV, $\langle S_1S_2\rangle = \langle S_1S_3\rangle = \langle S_2S_3\rangle$, the spin blockage appears, which can be used to discuss the chiral circulation measurement. However, when $t/t_0 > 1$, with the distance between side QDs closer, both the spins become AFM coupling due to the Pauli repulsion interaction, while decoupling will occur between QD_1 and $QD_{2/3}$ with larger t, that is, $\langle S_1S_2\rangle = \langle S_1S_3\rangle = 0, \langle S_2S_3\rangle < 0$. With increasing t_0 to 0.35 meV, the interdot repulsion interaction and FM coupling in the initial linear chain are stronger, which shows that $\langle S_2S_3\rangle$ is greater than $t_0 = 0.15$ meV at $t = 0$ meV. At $t = t_0 = 0.35$ meV, the kink point also appears, while QD1 reaches approximate decoupling at a larger t ($t \gg t_0 = 0.35$ meV).

3.2. Asymmetry TTQDs, $t_{12} \neq t_{13}$

Next, we consider the case of asymmetric TTQDs by setting $t_{12} \neq t_{13}$, as shown in Fig. 3(a). When the coupling strength between QD_1 and QD_2 changes to $t_{12} = 0.15$ meV and $t_{12} = 0.3$ meV under $V = 0$ mV and other parameters are the same as those discussed above, the transition of spin correlation with t is shown by $\langle S_1S_2\rangle \neq \langle S_1S_3\rangle$, due to the broken mirror symmetry. The overall $\langle S_iS_j\rangle$ will appear in two intersections, the first one appears at $t = t_{12} = 0.15$ meV, $\langle S_1S_2\rangle = \langle S_2S_3\rangle$, and the second at $t = t_{13} = 0.25$ meV, $\langle S_1S_3\rangle = \langle S_2S_3\rangle$.

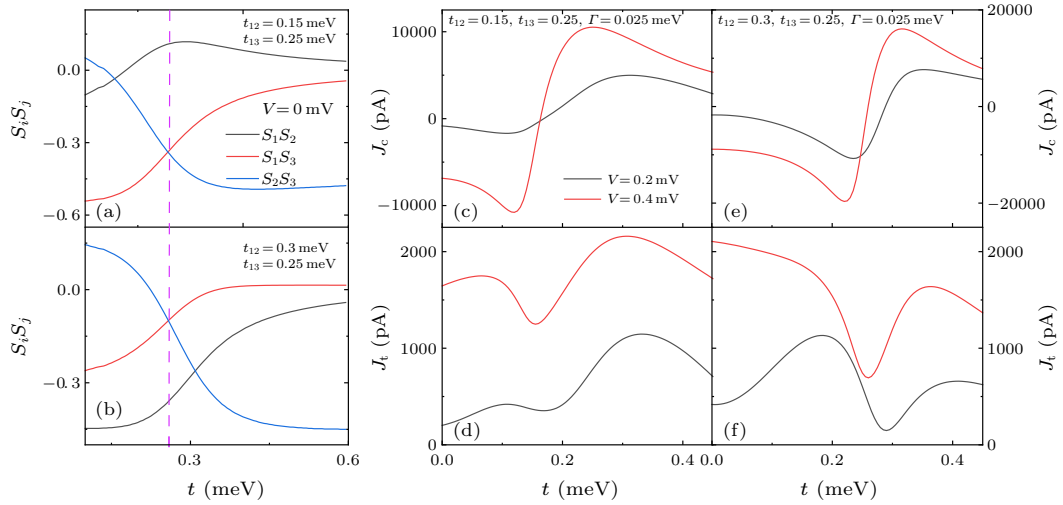


Fig. 3. The system presents an asymmetric configuration, in which the coupling strength between QD_1 and QD_2 is changed so that $t_{12} \neq t_{13}$. When $V = 0$ mV, the spin correlation coefficient $\langle S_iS_j\rangle$ (i, j = 1–3) changes with the coupling strength t, keeping $t_{13} = 0.25$ meV, for $t_{12} = 0.15$ meV in (a) and $t_{12} = 0.3$ meV in (b). Due to the asymmetric structure, $\langle S_1S_2\rangle$ and $\langle S_1S_3\rangle$ no longer overlap. [(c), (d)] J_c and J_t of the configuration with t when $V = 0.2$ mV and 0.4 mV, while the situation of in configuration (b) is shown in (e) and (f).

In this asymmetric structure, the internal chiral circulation and J_t also undergo blockage changes, as shown in Figs. 3(c) and 3(d). When the bias $V = 0.2$ mV is relatively small, the inversion of J_c appears at $t = t_{13} = 0.25$ meV (black line), at $t < t_{13} = 0.25$ meV the chiral circulation shows CW, $J_c < 0$. When $t = t_{13}$, the two chiral states have the same occupancy probability $J_c = 0$, while at $t > t_{13}$ the dominant chiral state overturns and the circulation changes to CCW, $J_c > 0$. As the voltage increases to $V = 0.4$ mV, the spin blockage is transformed into $t = t_{12} = 0.15$ meV, and the chiral circulation inversion will also occur around $t = 0.15$ meV (red line).

When t_{12} increases up to $t_{12} = 0.3$ meV and $t_{13} = 0.25$ meV remains unchanged, the overall spin correlation and internal circulation change with t as shown in Fig. 3(b). For the second intersection at $t = t_{13} = 0.25$ meV, $\langle S_1S_3\rangle = \langle S_2S_3\rangle$ remains unchanged, and the above transition shifts to $t = t_{12} = 0.3$ meV, $\langle S_1S_2\rangle = \langle S_2S_3\rangle$. If t_{12} transforms at constant t_{13} to destroy the mirror triangle structure, the difference of spin correlation crossing only appears in $\langle S_1S_2\rangle$ with a constant immobile transformation of $\langle S_1S_3\rangle$. However, the J_c flip to $t = t_{12} = 0.3$ meV at $V = 0.2$ mV, and when $V = 0.4$ mV, the inversion will change into $t = t_{13} = 0.25$ meV, which is different from $t_{12} < t_{13}$ shown in Figs. 3(e) and 3(f). This phenomenon may be due to the relative tunnelling coupling of transmission path. As one path circulation rate increases, the influence of the bias may make one of the paths easier to transport electrons, thus affecting the conversion of kinks in the asymmetric TTQDs structure at different biases.

3.3. Influence of dot–lead coupling on symmetric TTQDs

In this section, we discuss the influence of dot–lead coupling strength (Γ) on chiral circulation J_c and J_t. In order to simplify and keep TTQDs in the mirror symmetry, the parameters $t_{12} = t_{13} = t_0 = 0.25$ meV and $\varepsilon = -U/2 = -0.5$ meV are set unchanged to maintain particle-hole symmetry. When $V = 0.4$ mV, the characteristics of J_c and J_t with the coupling strength t of $QD_{2/3}$ at different Γ are shown in Figs. 4(a) and 4(b). With the increase of Γ, the conversion of J_c is fixed at $t = t_0$, which indicates that the inversion of the chiral circulation and the dominant chiral states in the TTQDs remain un-

changed with Γ. The chiral term $\hat{S}_1 \cdot (\hat{S}_2 \times \hat{S}_3)$ composed by three spins is a strong spin frustration phenomenon, in which internal chirality will not be affected by the external electronic reservoir fluctuation. However, the overall transformation of J_c becomes more gentle with Γ, and the extremum will gradually deviate $t = t_0$, at which the blockage of J_t will gradually disappears. For example, when Γ is 0.005 meV, the maximum point appears at $t = 0.265$ meV, and when the coupling strength gradually increases to $\Gamma = 0.3$ meV, the maximum point becomes 0.36. At $\Gamma = 0.6$, the J_c^{max} occurs at $t = 0.48$ meV.

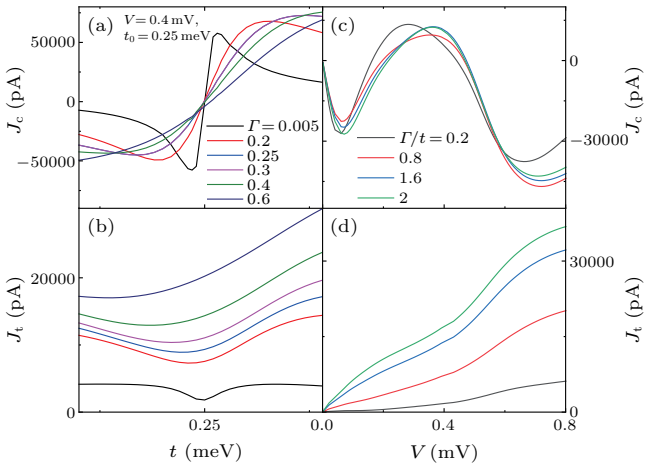


Fig. 4. [(a), (b)] In the symmetrical TTQDs configuration, $t_{12} = t_{13} = t_0 = 0.25$ meV, chiral current J_c and J_t are as functions of t with different dot–lead coupling $\Gamma = 0.005, 0.2, 0.25, 0.3, 0.4, 0.6$ meV, under $V = 0.4$ mV. [(c), (d)] J_c and J_t versus bias V for $\Gamma/t = 0.2$, 0.8, 1.6, and 2.

As the dot–lead coupling strength is relatively smaller ($\Gamma = 0.005$ meV), J_c and J_t show three obvious distribution regions. For a small coupling ($t/t_0 < 1$), $J_c < 0$ corresponds to the CW circulation direction, but at a larger coupling strength ($t/t_0 > 1$), the sign of J_c is reversed, indicating the CCW. For the symmetric structure near the transition state ($t/t_0 = 1$), the chiral current shows a huge jump near the kink point, and the extreme value of J_c can reach about ± 16 at $t \approx t_0$. When $\Gamma = 0.6$, J_t progressively increases with t, and the blockage is overcome, indicating the transmission path of left-QD_2–QD_3-right lead become accessible, and J_t will not be affected by the internal blockage of TTQDs chirality. The extreme value point also becomes far away from t_0 (at $t = 0.48 \gg t_0$), and the overall change trend will be much slower.

We also investigate the variation of J_c and J_t with bias in an equilateral symmetric TTQDs system ($t = t_0 = 0.25$ meV) at different Γ/t, as shown in the Figs. 4(c) and 4(d). With the increase of Γ/t, the chirality circulation is still CW in blocking region (0 mV $< V <$ 0.15 mV) and CCW in the coexistence region (0.15 mV $< V <$ 0.45 mV). At the same time, J_t shows a positive correlation and a persistent increase with bias and Γ.

In order to illustrate the physical mechanism caused by internal spin gauge field, we calculated the spin correlation $\langle S_i S_j \rangle$ as a function of the interdot interaction t for $\Gamma =$ 0.05 meV and 0.6 meV at $V = 0$ and $V = 0.4$ mV, as shown in Figs. 5(a)–5(d).

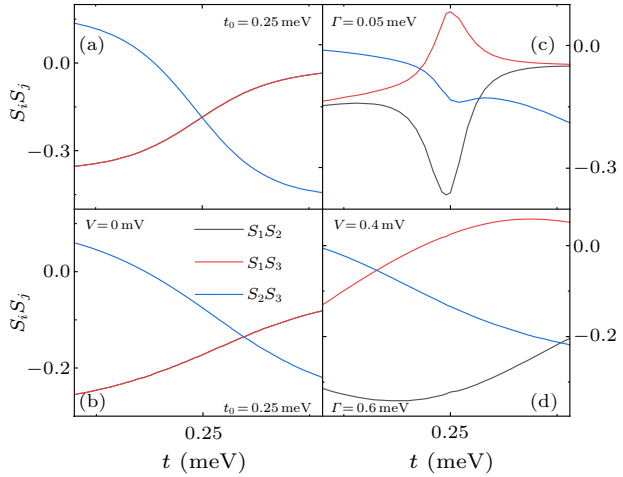


Fig. 5. Under different dot–lead coupling $\Gamma = 0.005$ meV and 0.6 meV, the spin correlation coefficient $\langle S_i S_j \rangle$ ($i, j =$ 1–3) as a function of t between QD_2 and QD_3 at $V = 0$ mV in (a) and (b). Adding biases at $V = 0.4$ mV are demonstrated in (c) and (d).

When $V = 0$ mV the dot–lead coupling strength is relatively smaller ($t_0 \gg \Gamma = 0.05$ meV), spin-dependent blockage still occurs at $t = t_0 = 0.25$ meV, $\langle S_1 S_2 \rangle = \langle S_1 S_3 \rangle = \langle S_2 S_3 \rangle$. As $t < t_0$, the spins on QD_2 and QD_3 demonstrate to FM coupling, the spin correlation $\langle S_2 S_3 \rangle > 0$, while the spins transform into AFM interaction and QD_1 is gradually decoupled from $QD_{2/3}$ at $t > t_0$, $\langle S_2 S_3 \rangle < 0$, and $\langle S_1 S_2 \rangle = \langle S_1 S_3 \rangle = 0$, similar to the case of $\Gamma = 0.025$ meV. For $\Gamma = 0.6$ meV, the spin frustration will appear at $t = 0.3$ meV, $\langle S_1 S_2 \rangle = \langle S_1 S_3 \rangle = \langle S_2 S_3 \rangle$ deviates from the blockage at $t_0 = 0.25$ meV, which means that the hybridization will affect spins on $QD_{2/3}$, causing the internal blocking changes to larger t. This is the result of competition between the internal circulation and the conduction path of left-QD_2–QD_3-right lead. When we gradually increase the coupling strength Γ, the spin correlation blockage will shift slightly, but due to the equilateral triangular symmetry inside the TTQDs system, the overall circulation and kink point do not transfer significantly.

As adding bias to TTQDs at $V = 0.4$ mV, it manifests $\langle S_1 S_2 \rangle \neq \langle S_1 S_3 \rangle$, attributed to the bias to break the spin correlation symmetry. At $\Gamma = 0.05$ meV, the blockage is still at $t = t_0 = 0.25$ meV. As $\Gamma = 0.6$, the internal chiral circulation will be weakened due to the strong dot–lead hybridization Γ, the spin-correlation kink and blockage disappear. With t increasing, QD_2 and QD_3 gradually approach with a continuous AFM coupling interaction. $\langle S_2 S_3 \rangle$ presents an approximate linear decline without transition and QD_1 is decoupled at larger t (at $t = 0.8$ meV, $\langle S_1 S_{2/3} \rangle = 0$). This shows that the Γ has little effect on the circulation response of external bias excitation, which only affects the conduction of J_t

in the transport path but nothing works for the chirality correlation inside the TTQDs.[46] $\hat{S}_1 \cdot (\hat{S}_2 \times \hat{S}_3)$ has robust anti-interference and can stably exist in various quantum devices and qubit applications.[47–49]

4. Conclusions

In conclusion, we have investigated the relationship between symmetry and spin frustration in TTQDs. By gradually increasing the coupling interaction t between the side-dots in LTQDs, the internal chiral circulation and blockage will be generated, and the direction of the J_c will change with t. When we change the coupling strength t_{ij} $(i, j = 1–3)$ or symmetric configuration of the initial LTQDs, the internal spin gauge field will also transform, corresponding to the spin correlation and chiral circulation inversion.

In addition, when we vary the external dot–lead coupling, the internal chiral interaction will compete with the J_t, but has little effect on the internal blocking. This indicates that the internal chiral circulation has strong resistance to external interference and stability. The chiral term $\hat{S}_1 \cdot (\hat{S}_2 \times \hat{S}_3)$ existing in TTQDs can be qualitatively regulated by external bias and internal chiral structure, which can be further applied to the integration and regulation of quantum gates and quantum computers.

Acknowledgements

This work was supported by the National Natural Science Foundation of China (Grant Nos. 12274454, 11774418, 11374363, 11674317, 11974348, 11834014, and 21373191), the Strategic Priority Research Program of CAS (Grant Nos. XDB28000000 and XDB33000000), the National Natural Science Foundation of China (Grant No. 11974348), the Training Program of Major Research Plan of NSFC (Grant No. 92165105), and the Outstanding Innovative Talents Cultivation Funded Programs 2023 of Renmin University of China. The computational resource was provided by the Physical Laboratory of High Performance Computing at Renmin University of China.

References

[1] Hou Z, Zhang Q, Zhang X, *et al.* 2020 *Adv. Mater.* **32** 1904815
[2] Iwasaki J, Mochizuki M and Nagaosa N 2013 *Nat. Commun.* **4** 1463
[3] Zhang X, Xia J, Zhou Y, Liu X, Zhang H and Ezawa M 2017 *Nat. Commun.* **8** 1717
[4] Psaroudaki C and Panagopoulos C 2021 *Phys. Rev. Lett.* **127** 067201
[5] Lee P A 2007 *t-j model and the gauge theory description of underdoped cuprates*. In: *Handbook of High-Temperature Superconductivity* (Berlin: Springer) p. 527
[6] Hsieh C Y, Rene A and Hawrylak P 2012 *Phys. Rev. B* **86** 115312
[7] Wang Y, Zhu Z, Wei J and Yan Y 2020 *Europhys. Lett.* **130** 17003
[8] Scarola V and Sarma S D 2005 *Phys. Rev. A* **71** 032340
[9] Ward D R, Kim D, Savage D E, Lagally M G, Foote R H, Friesen M, Coppersmith S N and Eriksson M A 2016 *npj Quantum Inf.* **2** 16032
[10] Gimenez I P, Hsieh C Y, Korkusinski M and Hawrylak P 2009 *Phys. Rev. B* **79** 205311
[11] Saraga D S and Loss D 2003 *Phys. Rev. Lett.* **90** 166803
[12] Mitchell A K and Logan D E 2010 *Phys. Rev. B* **81** 075126
[13] Akagi Y and Motome Y 2010 *J. Phys. Soc. Jpn.* **79** 083711
[14] Koga M, Matsumoto M and Kusunose H 2014 *J. Phys. Soc. Jpn.* **83** 084707
[15] Liang W, Shores M P, Bockrath M, Long J R and Park H 2016 *Nature* **417** 725
[16] Tatara G and Kawamura H 2002 *J. Phys. Soc. Jpn.* **71** 2613
[17] Tatara G and Kohno H 2003 *Phys. Rev. B* **67** 113316
[18] Tatara G, Kohno H and Shibata J 2008 *Phys. Rep.* **468** 213
[19] Tatara G 2019 *Physica E* **106** 208
[20] Xiao D, Chang M C and Niu Q 2010 *Rev. Mod. Phys.* **82** 1959
[21] Taguchi K and Tatara G 2009 *Phys. Rev. B* **79** 054423
[22] Zhang S S, Ishizuka H, Zhang H, Halász G B and Batista C D 2020 *Phys. Rev. B* **101** 024420
[23] Hsieh C Y, Rene A and Hawrylak P 2011 *Phys. Rev. B* **86** 115312
[24] Liu Y M, Wang Y D and Wei J H 2022 *Chin. Phys. B* **31** 057201
[25] Cheng Y, Wang Y, Wei J, Zhu Z and Yan Y 2017 *Phys. Rev. B* **95** 155417
[26] MacDonald A H, Girvin S and Yoshioka D 1988 *Phys. Rev. B* **37** 9753
[27] Qi Y, Liu Y M, Wang Y D, Wei J H and Zhu Z G 2023 *Chin. Phys. B* **32** 087304
[28] Vernek E, Büsser C, Martins G, Anda E, Sandler N and Ulloa S 2009 *Phys. Rev. B* **80** 035119
[29] Koga M, Matsumoto M and Kusunose H 2012 *J. Phys. Soc. Jpn.* **81** 123703
[30] Oguri A, Amaha S, Nishikawa Y, Numata T, Shimamoto M, Hewson A and Tarucha S 2011 *Phys. Rev. B* **83** 205304
[31] Lorke A, Kotthaus J and Ploog K 1990 *Phys. Rev. Lett.* **64** 2559
[32] Childress L, Sørensen A and Lukin M D 2004 *Phys. Rev. A* **69** 042302
[33] Shim Y P 2022 *J. Appl. Phys.* **132** 064402
[34] Liu Y, Chen Y and Wang Z 2010 *Solid State Commun.* **150** 1136
[35] Li Z, Cheng Y, Wei J, Zheng X and Yan Y 2018 *Phys. Rev. B* **98** 115133
[36] Li Z, Tong N, Zheng X, Hou D, Wei J, Hu J and Yan Y 2012 *Phys. Rev. Lett.* **109** 266403
[37] Hou D, Wang R, Zheng X, Tong N, Wei J and Yan Y 2014 *Phys. Rev. B* **90** 045141
[38] Byers N and Yang C 1961 *Phys. Rev. Lett.* **7** 46
[39] Li Z H, Tong N, Zheng X, Hou D, Wei J, Hu J and Yan Y 2009 *Phys. Rev. Lett.* **109** 266403
[40] Okamoto J I, Mathey L and Haertle R 2016 *Phys. Rev. B* **94** 235411
[41] Hu J, Luo M, Jiang F, Xu R X and Yan Y J 2011 *J. Chem. Phys.* **134** 101106
[42] Feynman R P and Vernon F L 2000 *Ann. Phys.* **281** 547
[43] Feynman R P and Jr F V 1987 *Ann. Phys.* **281** 547
[44] Jin J, Zheng X and Yan Y 2008 *J. Chem. Phys.* **128** 234703
[45] Ye L Z, Wang X, Hou D, Xu R X, Zheng X and Yan Y 2011 *WIR Comput. Mol. Sci.* **133** 101106
[46] Waugh F, Berry M, Mar D, Westervelt R, Campman K and Gossard A 1995 *Phys. Rev. Lett.* **75** 705
[47] Xia J, Zhang X, Liu X, Zhou Y and Ezawa M 2023 *Phys. Rev. Lett.* **130** 106701
[48] Weymann I, Bułka B and Barnaś J 2011 *Phys. Rev. B* **83** 195302
[49] Łuczak J and Bułka B R 2017 *Quantum Inf. Process.* **16** 10